Chapter 34
Evolution on the Asymptotic Giant Branch

34.1 Nuclear Shells on the Asymptotic Giant Branch

In stars of low and intermediate mass, i.e. in stars of initial mass $\lesssim 8\,M_\odot$, the phase following the end of core helium burning is of special interest. It is characterized by the presence of two nuclear burning shells around a carbon-oxygen core, of which one–the helium shell–is thermally unstable. Stars in this mass range and phase of the evolution populate the so-called *asymptotic giant branch* (AGB), previously also known as "second-ascent branch". In this chapter we give an overview over the important physical effects which are characteristic for AGB stars. As we will see, the evolution is highly complicated and the numerical models far from being perfect. For more details and a much more thorough discussion, we refer the reader to the review by Herwig (2005) and to the textbook by Habing and Olofsson (2003). The classical review by Iben and Renzini (1983) is still worth being studied, too.

After the end of core helium burning and after the hydrogen shell has burned outwards for some time, the temperature in this shell drops, and hydrogen-shell burning extinguishes. This phase of the evolution is often called the *early AGB* (E-AGB). The layer of transition between the hydrogen-rich envelope and the region of helium stays now at a fixed value of m. In stars above $M \approx 4\,M_\odot$ convection may reach below the H–He discontinuity and mix more ashes of hydrogen shell burning to the surface. This is the *second dredge-up* we already encountered in Chap. 31. But there is still the active helium-burning shell moving to higher values of m and therefore approaching the bottom of the hydrogen-rich envelope. Since helium burning proceeds at a temperature of $\gtrsim 10^8$ K, which is about ten times the temperature of hydrogen ignition, hydrogen burning starts again, and once more there are two shell sources. In this phase, shell burning becomes secularly unstable, resulting in a thermal runaway. This leads to a cyclic phenomenon (reoccurring here within some 10^4–10^5 years) known as *thermal pulses (TP).* Their general properties will be discussed in Sect. 34.3 in connection with their appearance in intermediate-mass stars where the unstable shells initially are in the deep interior, and the response of the surface is moderate. In the case of low-mass stars, the

R. Kippenhahn et al., *Stellar Structure and Evolution*, Astronomy and Astrophysics Library, DOI 10.1007/978-3-642-30304-3_34,

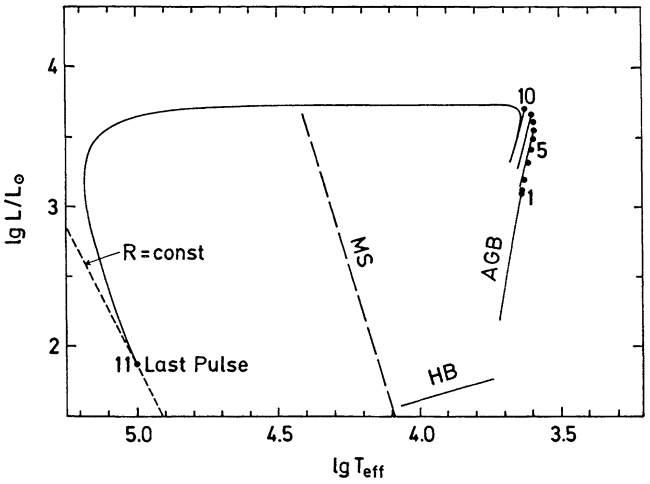

Fig. 34.1 Schematic evolutionary track of a star of $0.6M_{\odot}$ ($X_{\rm H} = 0.749$, $X_{\rm He} = 0.25$) for the phases after central helium burning. The model moves upwards along the asymptotic giant branch (AGB) until thermal pulses occur (indicated by *full circles*). The changes during a pulse are shown only for pulse 9 and pulse 10. Before the last pulse (11), for which only the onset is shown, the track has reached the white-dwarf area of the HR diagram. The main sequence (MS), the horizontal branch (HB), and a line of constant radius in the white-dwarf region are indicated (after Iben and Renzini 1983)

luminosity and the surface temperature can vary appreciably with each pulse. This is the more pronounced the less mass is left above the unstable shells, as we will see in Sect. 34.7. If a thermal pulse occurs in certain critical phases (with neither too much nor too little mass above the shells) the models can even move rapidly through large regions of the HR diagram (Kippenhahn et al. 1968; Schönberner 1979). The evolution displayed in Fig. 34.1, shown as an illustrative example and taken from the review article "Asymptotic Giant Branch Evolution and Beyond" by Iben and Renzini (1983) goes through 11 pulses, the onsets of which are indicated by heavy dots. The variation of the surface values is not very pronounced, since there is enough mass above the nuclear shells to damp the changes caused by the instability. This phase is also called the *thermally pulsing AGB* (TP-AGB) to discriminate it from the E-AGB.

The pulses are more or less an envelope phenomenon and are of no influence on the core. The inner part of the CO-core resembles more and more a white dwarf. Only the hydrogen-rich envelope, small in mass but thick in radius, at first gives the star the appearance of a red giant. After the envelope mass has dropped below, say, one per cent, the envelope starts to shrink. With decreasing envelope mass the star moves typically within a few thousand to 10^4 years to the left of the main sequence (see Fig. 34.1). This is the *post-AGB* phase. Then shell burning extinguishes and the star becomes a white dwarf. In the case shown, the star experiences a final thermal pulse (11), which will lead to large excursion in the HRD. This will be discussed further in Sect. 34.9.

It is clear that the mass in the envelope is diminished by two effects: the hydrogen burning at the bottom and mass loss from the surface. Therefore the stage at which the star leaves the asymptotic branch, turning to the left, is sensitive also to the amount of mass loss in the red giant phase. This influences the mass of the final white dwarf (cf. Sect. 35.2) and limits the number of thermal pulses (see Sect. 34.6).

34.2 Shell Sources and Their Stability

Stars on the AGB are the first to have more than one nuclear shell. Their productivity may change considerably and even go to zero for some time. Neighbouring shell sources can influence each other, since each type of burning requires a separate range of temperature. For example, if a helium shell source operating at roughly 2×10^8 K approaches a hydrogen-rich layer, we can expect an enormous increase of hydrogen burning, which usually proceeds at $T \lesssim 3 \times 10^7$ K. It is also clear that different shell sources will generally move with different "velocities" $\dot{m}_i$ through the mass, unless their contributions L_i to the total luminosity are in certain ratios. If X_i denotes the mass concentration of the reacting element ahead of the shell source, and q_i the energy released by the fusion of one unit of mass, then $\dot{m}_i = L_i/(q_i X_i)$. For example, on the AGB, the relative motion of the hydrogen and helium shell sources through the mass is given by the ratio

$$\frac{\dot{m}_\mathrm{H}}{\dot{m}_\mathrm{He}} = \frac{L_\mathrm{H}}{L_\mathrm{He}} \frac{q_\mathrm{He}}{q_\mathrm{H}} \frac{X_\mathrm{He}}{X_\mathrm{H}}. \tag{34.1}$$

This gives a stationary situation with roughly equal velocities only if $L_\mathrm{H} \approx 7 L_\mathrm{He}$, since typically $X_\mathrm{H} \approx 0.7$, $X_\mathrm{He} \approx 1$, and $q_\mathrm{H}/q_\mathrm{He} \approx 10$. Otherwise the two shell sources approach each other or the inner one falls behind.

Shell-source models for several evolutionary phases can be approximated well by solutions obtained by assuming complete equilibrium. While burning outwards, a shell source has the tendency to concentrate the reactions over steadily decreasing mass ranges. One then has to deal with rather short *local* nuclear time scales, defined as those time intervals in which the burning shifts the very steep chemical profile over a range comparable to its own extension. This would require computations of tens of thousands models with very short time steps, if it were not for the influence of mass loss (see Sect. 34.6).

All changes become much more rapid, and the assumption of complete equilibrium certainly has to be dropped if the shell source is thermally unstable. The reasons for such instabilities will be made plausible by considering a very simple model for the shell source and its perturbation. The procedure is completely analogous to that used in Sect. 25.3.5 for the stability of a central nuclear burning. The only difference between the two cases is that the burning regions are geometrically different and the density reacts differently to an expansion.

Let us compare the two cases of a central burning and a shell-source burning in Fig. 34.2. In the central case, the mass of the burning region is $m \sim \varrho r^3$, and an

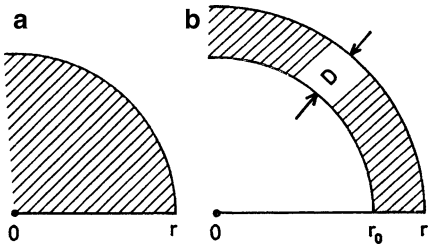

Fig. 34.2 The main region of nuclear energy production (*hatched*) in the cases of (**a**) central burning and (**b**) shell source burning

expansion $dr > 0$ with $dm = 0$ requires a relative change of the density [compare with (25.25)]

$$\frac{d\varrho}{\varrho} = -3\frac{dr}{r}. \tag{34.2}$$

In the case of a shell source of thickness D, we write the upper boundary of the burning region as $r = r_0 + D$ (cf. Fig. 34.2b). For relatively small D the mass in the burning shell is $m \sim \varrho r_0^2 D$. If the burning region expands with roughly $r_0 =$ constant as a reaction to an energy perturbation, we have $dr = dD$, and the condition $dm = 0$ now leads to

$$\frac{d\varrho}{\varrho} = -\frac{dD}{D} = -\frac{r}{D}\frac{dr}{r}. \tag{34.3}$$

We now assume that the mass outside $r_0 + D$ expands or contracts homologously. Then for the pressure in the shell we can use the relation $dP/P = -4dr/r$ as in (25.25). When comparing (34.3) with (34.2) we see that we only have to replace the factor 3 by the factor r/D when going from the central case to that of a shell source. This can be done directly in expression (25.29) for the gravothermal heat capacity c^*. For simplicity we neglect the perturbation of the flux dl_s and have from (25.30)

$$c^*\frac{dT}{dt} = d\varepsilon\,; \quad c^* = c_P\left(1 - \nabla_{\mathrm{ad}}\frac{4\delta}{4\alpha - r/D}\right). \tag{34.4}$$

(Note that the time derivative dT/dt represents a differential perturbation; it could be replaced by $d(dT/dt)$ since $T = T_0 + dt$ with time-independent T_0.) If c^* is positive, then the shell source is unstable, since an additional energy input ($d\varepsilon > 0$) leads to higher T and further increased burning.

We first recover the well-known flash instability in the case of strong degeneracy of the electron gas with $\delta \to 0$. Indeed we have seen in Chap. 33 that the helium flash occurs in a shell rather than in the centre if the central part is cooled by neutrino emission.

In addition, (34.4) shows that there is a new instability which can occur even for an ideal monatomic gas ($\alpha = \delta = 1, \nabla_{\mathrm{ad}} = 2/5$) and which has no counterpart in the case of central burning. It depends only on the geometrical thickness D of the shell source. If D/r is small enough (in our simple representation smaller than 1/4),

c^* is positive and the shell source is secularly unstable. This instability of a shell source is called *pulse instability* for reasons which will become obvious very soon.

It is amazing that such a simple geometrical property can cause a thermal instability, though it becomes more plausible if we consider the change of the pressure in the shell source as a hydrostatic reaction to the lifting of the layers above (for which we simply assume homology). Suppose that the shell tries to get rid of the perturbation energy by expansion. A substantial relative increase of the thickness $dD/D > 0$ gives the same absolute value for the relative decrease of the density $d\varrho/\varrho < 0$, but only a very small relative increase dr/r, if $D/r \ll 1$ [cf. (34.3) and Fig. 34.2b]. This means that the layers above are scarcely lifted, so that their weight remains about constant and hydrostatic equilibrium requires $dP/P \approx 0$. In fact with the homology relation $dP/P = -4dr/r$ and (34.3) we find the connection between dP and $d\varrho$ to be

$$\frac{dP}{P} = 4\frac{D}{r}\frac{d\varrho}{\varrho}. \tag{34.5}$$

Considering the equation of state

$$\frac{d\varrho}{\varrho} = \alpha\frac{dP}{P} - \delta\frac{dT}{T}, \tag{34.6}$$

we see that expansion ($d\varrho/\varrho < 0$) necessarily leads to an *increase* of the temperature ($dT/T > 0$), since $dP/P \to 0$ for $D/r \to 0$:

$$\frac{d\varrho}{\varrho} = -\delta\frac{dT}{T}. \tag{34.7}$$

Therefore the expansion of a thin shell source does not stabilize it, but rather enforces the liberation of energy by heating. This means that the shell source reacts just as if the equation of state were $\varrho \sim 1/T$, which, of course, gives instability [cf. (34.4) with $\alpha = 0$ and $\delta = 1$].

While the foregoing discussion provides the main points correctly, it can easily be completed by also considering the perturbation of the local luminosity. Then some of the surplus energy can flow away, and instability requires, in addition, that the temperature sensitivity of the burning exceeds a certain limit, which is usually fulfilled. The eigenvalue analysis of such stellar models has shown that they are indeed thermally unstable and that the unstable modes are complex (Härm and Schwarzschild 1972).

The pulse instability was first found (Schwarzschild and Härm 1965) for a helium shell source in calculations for a $1M_\odot$ star. The same type of instability was encountered independently in a model for $5M_\odot$ during the two-shell phase, and here it turned out that the instability leads to nearly periodic relaxation oscillations, which were called *thermal pulses,* as described below (Weigert 1966). They are now known to be a genuine property of those low- and intermediate-mass stars, which are massive enough to ignite helium and evolve into the double-shell burning phase of the AGB.

A unified scheme for the stability of shell sources has been developed by Yoon et al. (2004). It includes the present case of geometrically thin shells as well as the flash instability of Sect. 33.4 and demonstrates that shells are more stable, if they are geometrically thick, non-degenerate, or hotter.

34.3 Thermal Pulses of a Shell Source

Thermal pulses occur in models containing one or more shell sources, and in stars of different masses and compositions. We start by describing their properties according to the calculation of the first six pulses in a $5\,M_\odot$ model, found for the first time in a star in this mass range by Weigert (1966). Although the physical details and numerical treatment of the models have changed a lot since then, the basic picture of thermal pulses is still the same. The instability occurs in the helium shell source after it has reached $m/M \approx 0.1597$. It then contributes only a little to the surface luminosity L, which is almost completely supplied by the nearby hydrogen shell source located at $m/M \approx 0.1603$.

The instability results immediately in a thermal runaway: the shell source reacts to the surplus energy with an increase in T, which enhances the release of nuclear energy, etc. The increase of T is connected with an expansion according to (34.7). This can be seen from Fig. 34.3a, b which give T and ϱ at maximum $\varepsilon_{\mathrm{He}}$ in the unstable shell source as functions of time (Note that the thermal runaway in a *flash* instability would proceed with $\varrho =$ constant.). Since helium burning has an extreme temperature sensitivity, the increase of T strongly enhances the productivity L_{He} of the shell source, in later pulses even to many times the surface value L. But most of this energy is used up by expansion of the layers above, and this expansion reduces considerably the temperature in the hydrogen shell source, such that L_{H} decreases significantly. After starting rather slowly the thermal runaway accelerates more and more until reaching a sharp peak within a few years. The helium shell source is now widely expanded and is therefore no longer unstable. The whole region then starts to contract again, which heats up the hydrogen shell source so that it regains its large productivity. Within a time of a few 10^3 years the whole region has asymptotically recovered its original overall structure, the helium shell source becomes unstable again and the next pulse starts. Figure 34.3 shows that the amplitude of the pulses and the time between consecutive pulses grows (in these calculations from 3,200 to 4,300 years). The reason for these changes is that the chemical composition around the shells changes considerably from pulse to pulse. Later calculations (for an early review, see Iben and Renzini 1983; for more recent results Wagenhuber 1996) showed that a nearly periodic behaviour is usually reached after roughly 20 pulses. The amplitude of a pulse has then become so large that during the maximum L_{He} exceeds L by orders of magnitude. The changes of the chemical composition still provide a small deviation from periodicity. Otherwise we would expect strictly periodic relaxation oscillations, i.e. the solution would have reached a limit cycle.

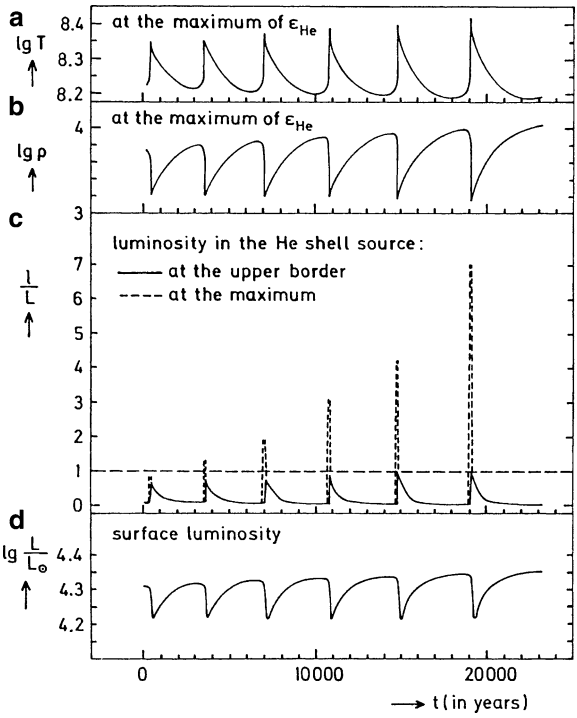

Fig. 34.3 Thermal pulses of the helium shell source in a $5M_\odot$ star after central helium burning. For the first six pulses, some characteristic functions are plotted against time from the onset of the first pulse. T is in K, ϱ in $\mathrm{g\,cm^{-3}}$ (After Weigert 1966)

The surface luminosity (Fig. 34.3d) drops in each pulse by typically $\Delta \lg L \approx 0.1 \ldots 0.2$ for models with rather massive outer envelopes. The visible reaction of the surface is much more pronounced if the pulses occur in a shell source close to the surface. Such models can move quite spectacularly through the HR diagram (compare with Sect. 34.9).

The properties of the thermal pulses depend on the type of star in which they occur. The cycle time τ_p (between the peaks of two consecutive pulses) becomes smaller with increasing mass M_c of the degenerate CO-core inside the helium shell source. From a large sequence of calculations Paczyński (1975) derived the following rough relation:

$$\lg\left(\frac{\tau_\mathrm{p}}{1\mathrm{year}}\right) \approx 3.05 + 4.50\left(1 - \frac{M_\mathrm{c}}{M_\odot}\right). \tag{34.8}$$

For $M_\mathrm{c} \approx 0.5M_\odot$ the cycle time is of the order of 10^5 years, while near the limit mass $M_\mathrm{c} \approx 1.4M_\odot$ it would be of the order of 10 years only. We now consider the number of pulses that can occur until M_c has reached 1.4 $M_\odot$. Suppose that the hydrogen shell source moves outwards by Δm per cycle time and produces most of the energy $L\tau_p$. Although $L \sim M_\mathrm{c}$ (cf. Sect. 34.4), Δm decreases strongly with growing M_c owing to the decrease of τ_p. One can estimate that, depending on the

details of the model, the total number of pulses (determined mainly by the very small τ_p in the last phases) must be $8,000 \ldots 10,000$ before $M_c \approx 1.4 M_\odot$. Of course, the shell source cannot burn further than to within a few $10^{-3} M$ from the surface. Therefore the total number of pulses will be much smaller if the stellar mass is well below $1.4 M_\odot$, either originally or owing to mass loss. In low-mass stars one can expect only ten pulses or so, as seen, for instance, in Fig. 34.1. These, however, occur very close to the surface and can affect the observable values certainly much more than pulses of a shell source in the deep interior.

During a thermal pulse, the star changes quite rapidly, particularly in the layers of the shell sources. Consequently the calculations have to use short time steps (often of the order of 1 year), and the number of models to be computed per pulse is large (or order 10^3). Additionally the fact that the helium shell is thermally unstable implies that the models have to be calculated with high precision to prevent unwanted thermal runaways. This makes the calculations even more challenging, and in fact, AGB calculations still suffer from numerical problems. It is therefore clear that one cannot hope to compute straightforwardly through the whole phase of about 10^4 pulses in intermediate-mass stars. In reality this is–fortunately–never needed, as mass loss on the AGB reduces the envelope mass quickly enough to limit the number of TPs to a few tens.

For stars of small mass (originally or by mass loss) the situation is better. One can certainly calculate through all of the relatively few pulses that occur before such a star becomes a white dwarf.

34.4 The Core-Mass-Luminosity Relation for Large Core Masses

Since the direct computation of TP-AGB models is so difficult, one may try to suppress the pulses artificially by neglecting the time-dependent terms (ε_g) in the energy equation and computing models in complete equilibrium. This gives (hopefully) an average evolution which might suffice in order to describe the evolution of the central core, and therefore of the final fate of the star.

An alternative approach are the so-called *synthetic AGB models* (see, e.g., Renzini 1981, or Marigo et al. 1996), where the global properties of AGB stars are followed using fitting functions such as (34.8) for the pulse durations. Extensive analytical fitting functions were derived by Wagenhuber and Groenewegen (1998) for quantities such as the luminosity, the pulse duration and interpulse time, the core mass at the first pulse, and many more. These functions were derived by fitting them to numerical models and are valid for various masses and chemical compositions, but simpler versions can be derived analytically. This is particularly true for the important core-mass-luminosity relation on the AGB.

We have seen that medium-mass stars, after central helium burning, develop a degenerate CO-core which is separated from the hydrogen-rich envelope by a thin

helium layer. At its bottom there is helium-shell burning, which contributes only, say, 10 % to L. Most of the luminosity is produced in a hydrogen shell source at the bottom of the envelope. It is not too bad an approximation if we simply assume $L \approx L_{\mathrm{H}}$, the hydrogen luminosity generated above a condensed core of mass M_{c} and radius R_{c}. We also have seen that L increases with increasing M_{c} (giving the upwards motion along the asymptotic branch) and here face the same situation as for low-mass stars on the ascending giant branch. One can again derive the dependence of the properties of the shell on M_{c} and R_{c} by homology relations as in Sect. 33.2, assuming the simple power laws (33.2) for κ and ε. But since we are dealing with rather massive cores and high temperatures here, the radiation pressure cannot be neglected. We therefore have to replace (33.3) by

$$P = \frac{\Re}{\mu}\varrho T + \frac{\alpha}{3}T^4 = \frac{1}{\beta}\frac{\Re}{\mu}\varrho T. \tag{34.9}$$

If again we write in the neighbourhood of given P and T the equation of state as a power law, $\varrho \sim P^{\alpha}T^{-\delta}$, we know from (13.7) that $\alpha = 1/\beta, \delta = (4-3\beta)/\beta$. Therefore we have as equation of state

$$P \sim \varrho^{\beta}T^{4-3\beta}. \tag{34.10}$$

As in (33.4)–(33.7), we write the quantities ϱ, T, P, and l in the shell as powers of M_{c} and R_{c}. By the same procedure as in Sect. 33.2 we can derive equations for the exponents. For the sake of simplicity we restrict ourselves to the case $a = b = 0$ and obtain, instead of (33.22),

$$\begin{aligned}
\varphi_1 &= \frac{4-\nu}{N}, \quad \varphi_2 = \frac{\nu - 12 + 6\beta}{N},\\
\psi_1 &= \frac{1+n}{N}, \quad \psi_2 = \frac{2\beta - n - 3}{N},\\
\tau_1 &= \beta\varphi_1 + (4-3\beta)\varphi_1, \quad \tau_2 = \beta\varphi_2 + (4-3\beta)\varphi_2,\\
\sigma_1 &= \frac{4n+\nu}{N}, \quad \sigma_2 = \frac{3-\nu-3n}{N}\beta
\end{aligned} \tag{34.11}$$

with

$$N = (4-3\beta)(1+n) + (1-\beta)(\nu - 4). \tag{34.12}$$

For $\beta = 1$ the relations (34.11) and (34.12) agree with (33.22) and (33.23) for $a = b = 0$.

With increasing core mass, β in the shell must decrease strongly, as can be seen from the following considerations. From (34.9) and (34.10) we have

$$\beta \sim \frac{\varrho T}{P} \sim \varrho^{1-\beta}T^{-3(1-\beta)}. \tag{34.13}$$

If we here replace ϱ, T by (33.4) and (33.5), then the dependence of β on M_c, R_c is given by

$$\frac{d\ln\beta}{d\ln M_c} = (1-\beta)\left[(\varphi_1 - 3\psi_1) + (\varphi_2 - 3\psi_2)\frac{d\ln R_c}{d\ln M_c}\right]. \tag{34.14}$$

One may start from an initial model that has been computed by solving the stellar structure equations numerically. This gives initial values for M_c, R_c, L, and β. Starting from these initial values we want to integrate (34.14). For simplicity, let us take for the derivative on the right-hand side of (34.14) Chandrasekhar's mass-radius relation of white dwarfs, and for the exponents in the energy generation $n = 2,\ \nu = 14$. The result of such an integration is shown by a dotted line in Fig. 33.2. In the same way, (33.27) can be integrated with σ_1, σ_2 from (34.11) and $\beta(M_c)$ as derived from the solution of (34.14). This gives the solid curve in Fig. 33.2. In spite of all approximations used, the integrated curves illustrate clearly the essential points.

For small core masses, $\beta \approx 1$ and the relation (33.25) holds, giving a steep increase of L with M_c [$L \sim M_c^7$ after (33.26)]. For larger M_c, radiation pressure becomes more and more important and β decreases. This gives a much smaller slope of the $L(M_c)$ curve. Indeed in the limit $\beta = 0$ (34.11) gives $\sigma_1 = 1, \sigma_2 = 0$, independent of n and ν:

$$L \sim M_c. \tag{34.15}$$

The L-M_c relation has become extremely simple, and we do not have to worry about the correct R_c-M_c relation. Indeed from numerical models Paczyński (1970) derived

$$\frac{L}{L_\odot} = 5.92 \times 10^4 \left(\frac{M_c}{M_\odot} - 0.52\right) \tag{34.16}$$

as an interpolation formula for sufficiently large M_c. The corresponding formula by Wagenhuber and Groenewegen (1998) contains a linear term as well, but has additional correction terms which improve the fit also for low core masses and which take into account different metallicities of the models. It is therefore much more complicated than (34.16).

34.5 Nucleosynthesis on the AGB

We now turn to the change of the chemical composition by a combination of burning and convection. Figure 34.4 shows (with expanded scales) m against t during the peak of two pulses of the models by Weigert (1966). The high fluxes near the maximum of helium burning create a short-lived, pulse-driven intershell convection zone (ISCZ), which, in the later pulses of this calculation, comes very close to the H–He discontinuity. For a short time, almost the entire matter between the two shells

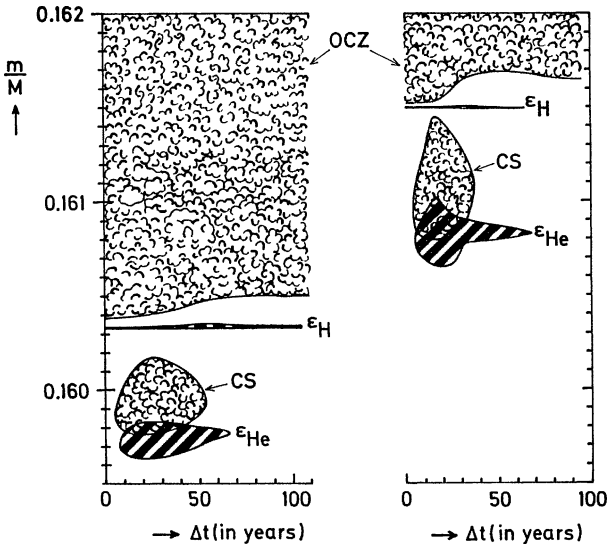

Fig. 34.4 Evolution of the mass shells around the two shell sources in a $5M_{\odot}$ star near the maxima of the first and sixth thermal pulses of the helium shell source (compare Fig. 34.3). The mass variable m is plotted against time, starting from an arbitrary zero point. Note the strongly expanded scales on both axes. *Cloudy* areas indicate the intershell convection zone (labelled here as CS) and the outer convective zone (OCZ); *hatched* areas show the regions of strongest nuclear energy production ($\varepsilon > 3 \times 10^7$ erg g^{-1} s^{-1}) (After Weigert 1966)

is mixed into the helium-burning shell, the products of which are spread over the intershell region. The outer convection zone (OCZ), which extends to the surface, can be seen to reach down nearly to the hydrogen shell source. The lower boundary of the OCZ moves during each pulse at first somewhat outwards, and then back again (compare also with Fig. 34.5, where the t axis is more compressed). Depending on mass, composition, and in particular on the assumption of mixing by convection or rotation, the ISCZ may even reach beyond the H–He discontinuity and dredge hydrogen into the intershell region but also enrich the outer layers with carbon. Similarly, the lower border of the OCZ can descend beyond the former location of the H–He discontinuity into the intershell region. Also in this case, hydrogen-rich material is transported downwards, while intershell material is dredged up by the OCZ and distributed over the whole outer envelope. This event is called the *third dredge-up*, and its reality is witnessed by the existence of carbon stars, stars on the AGB, in which the ratio of carbon-to-oxygen abundance is C/O > 1. In models with no mixing processes apart from convection according to the Schwarzschild criterion, the third dredge-up occurs only in stars of low mass and very low metallicity. This is not in agreement with observations, which found modifications of the surface composition also in more metal-rich and more massive stars. They can only be explained by the third dredge-up, and this requires additional mixing processes in the models, which could be overshooting or mixing induced by rotation. In Fig. 34.6

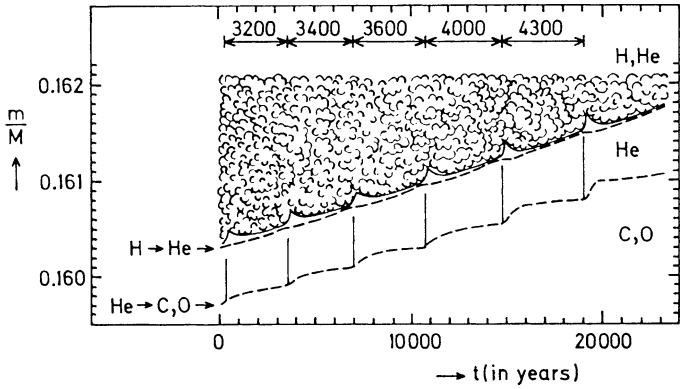

Fig. 34.5 Evolution of the mass elements around the two shell sources (*broken lines*) during the first six thermal pulses in a $5M_{\odot}$ star (compare Fig. 34.3). The "cloudy" area represents the outer convective zone (OCZ). The intershell convection zone (ISCZ) (labelled CS in Fig. 34.4) at the maximum of each pulse is so short-lived that it appears here as a vertical spike. The time (in years) between consecutive pulses is indicated at the *top* (After Weigert 1966)

we show a sketch of the sequence of mixing episodes leading to dredge-up and the formation of a so-called ^{13}C-pocket. In some models this additional mixing is added ad hoc with an efficiency tuned to reproduce the observations. The third dredge-up is one of the major problems of stellar evolution theory.

The mixing between layers containing protons and those burning helium at high temperatures is the beginning of interesting nucleosynthesis in stars on the AGB. Helium burning transforms ^{4}He into ^{12}C and ^{16}O, and the hydrogen shell source converts ^{16}O and ^{12}C into ^{14}N, which is left behind when the shell burns outwards between two pulses (between, e.g. t_3 and t_5 in Fig. 34.6). The ISCZ of the next pulse sweeps these ^{14}N nuclei down into the helium shell source where they are burned in the chain ^{14}N (α,γ) ^{18}F $(\beta^{+}\nu)^{18}$O $(\alpha,\gamma)^{22}$Ne. During a pulse in fairly massive stars, and therefore within the pulse-driven convective zone, the helium shell source attains a temperature so high that ^{22}Ne is also burned in the reaction ^{22}Ne $(\alpha,n)^{25}$Mg. This can provide a neutron source sufficiently strong to build up elements beyond the iron peak in the s-process (i.e. with neutron captures being *slow* compared with beta decay; see Sect. 18.7; Iben 1975; Truran and Iben 1977).

In other cases a corresponding neutron source may be provided by ^{13}C nuclei, which are burned via the chain ^{12}C (p,γ) ^{13}N $(\beta^{+}\nu)$ ^{13}C (α,n) ^{16}O in the helium shell. This happens, in contrast to the neon neutron source, between pulses and in a radiative environment (beginning at t_3 and t_6 in Fig. 34.6). For this neutron source to operate it is necessary to bring a sufficient amount of ^{13}C into the helium shell, which is achieved by mixing hydrogen-rich material from the envelope into the ^{12}C-rich region during the pulse phase in which the hydrogen-burning shell is extinguished (Fig. 34.6; $t_2 - t_3$). The protons are then captured by the ^{12}C nuclei to form ^{13}C. The region of high ^{13}C abundance is known as the ^{13}*C-pocket*, and will provide the neutron source later in the pulse cycle. According to theoretical models

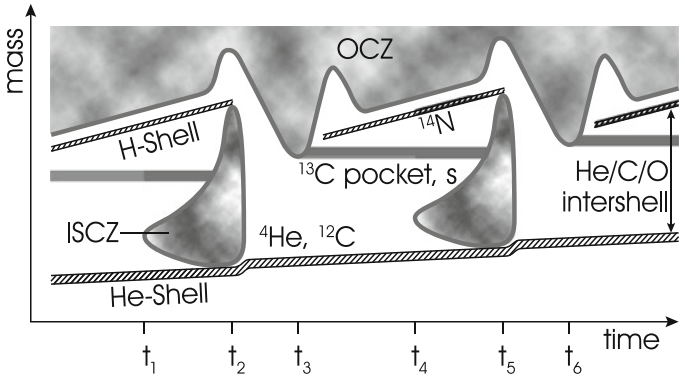

Fig. 34.6 Schematic sketch of the mixing episodes during thermal pulses, following similar representations in the reviews by Busso et al. (1999; Fig. 5) and Herwig (2005; Fig. 3). In contrast to Fig. 34.5, dredge-up is occurring here due to suitable assumptions about mixing processes, for example, due to the inclusion of overshooting. Shown is the region between the two shell sources and the bottom of the outer convection zone (OCZ). The mass scale is of order a few hundredths of a solar mass. At time t_1 the thermal pulse of the He-shell starts and triggers the intershell convection zone (ISCZ), which grows in mass and may reach the H-shell location at time t_2. The H-shell, however, has extinguished at this time due to the radial expansion of the intershell. After the pulse terminates, the OCZ can extend deeper than before (at t_3) and mixes both protons into the intershell as well as carbon, produced in the He-shell and transported upwards by the ISCZ, into the envelope. Upon contraction of the intershell, the OCZ recedes, the H-shell reignites, and the proton-enriched intershell layers heat to sufficiently high temperatures to allow $^{12}\mathrm{C}(p,\gamma)^{13}\mathrm{C}$ reactions in a radiative environment, forming the ^{13}C-*pocket*, which marks the start of s-process nucleosynthesis (see text; "s" in the figure). At t_4 the next pulse cycle starts, eventually leading to dredge-up of s-process elements and carbon to the surface of the AGB star. The interpulse time $t_4 - t_1$ is of order 10^4 years, the timescale $t_3 - t_1$ (or $t_6 - t_4$) is a few hundred years

this is the preferred neutron source in most AGB stars. Only in stars of higher mass the neon source may act as well. The main source for s-process elements appear to be AGB stars of lower mass. This is in agreement with theoretical models, which predict the third dredge-up to happen more easily in the lower mass range of AGB stars.

Such mixing and nuclear burning episodes may lead to modifications of the surface composition of AGB stars. We already mentioned that they may become enriched in carbon, initially produced in the helium shell, but subsequently mixed by the ISCZ and the OCZ to the surface. If a neutron source is operating and s-process elements are created, they, too, may appear at the photosphere. The detection of ^{99}Tc in the atmosphere of Mira variables (pulsating AGB stars) by Merrill (1952) proved the in situ production of this rare-earth element, as this isotope is unstable with a half-life time of only 211,000 years. Another signature of mixing between the convective envelope and nuclear burning regions is the presence of ^{19}F in AGB stars. It is created by the reaction $^{15}\mathrm{N}(\alpha,\gamma)^{19}\mathrm{F}$, which is taking place in the helium shell. The necessary production of ^{15}N can happen through different paths, one of them being $^{18}\mathrm{O}(p,\alpha)^{15}\mathrm{N}$ (see the neon neutron source, p. 428). Other

possibilities include the production of protons through (n, p)-exchange reactions, which therefore connects ^{19}F with the occurrence of the s-process and the presence of a neutron source.

Another modification of the surface composition, particularly of the ratio of ^{12}C to ^{14}N, can occur if the lower boundary of the OCZ becomes hot enough to start reactions of the CNO cycle. This event is known as *hot bottom burning (HBB)*, and occurs primarily in more massive AGB stars. It may even convert a carbon star back into an oxygen star (C/O < 1). The details of all these processes and their results are still rather uncertain, since they depend critically on the precise extensions of the two convective zones involved (the OCZ and the ISCZ) and on any other potential mixing process that may occur.

Nucleosynthesis on the AGB is very complex and depends on the details of mixing episodes and temperatures encountered. Due to the simultaneous presence of protons, α-particles, and possibly neutrons at temperatures of several 10^7 K up to $\approx 2 \times 10^8$ K, elements from C to Al are both produced and destroyed by proton and α captures. The primary production site is the helium shell, which creates C and O. If these elements encounter protons, ^{14}N will be the result. AGB stars can therefore be the source of primary nitrogen (*Primary* elements are produced directly from the basic building blocks, hydrogen and helium. *Secondary* elements, in contrast, are the result of nucleosynthesis of pre-existing heavier elements. An example would be the nitrogen resulting from CNO processes on the main sequence.). If ^{14}N is further exposed to α-particles in the helium shell, ^{18}O and then ^{22}Ne will result. In the more massive AGB stars, temperatures can be high enough for further α-captures, resulting in various Mg isotopes. Proton captures on Ne, Na, and Mg may change the isotope ratios and eventually lead to Al, including ^{26}Al, which has a half-life time of almost a million years. It decays under emission of 1.81 MeV γ-photons, contributing partially to the galactic γ-rays. Isotope ratios may further be modified by neutron capture reactions. ^{14}N, for example, acts as a so-called *neutron poison*, as it very effectively captures neutrons, thereby reducing the neutron flux needed for the s-process.

The detailed analysis of the abundances of these and the s-process elements is a very important way to learn about the internal evolution of AGB stars. An extensive discussion of nucleosynthesis in AGB stars can be found in the review by Lattanzio and Wood (in Habing and Olofsson 2003, p. 24). Chemical yields from AGB stars have been published by Karakas (2010), and Busso et al. (1999) reviewed in particular the s-process in AGB stars.

34.6 Mass Loss on the AGB

There is plenty of observational evidence that AGB stars suffer significant mass loss through stellar winds such that mass loss is, next to the thermal pulses, the second major factor determining the evolution on the AGB. Direct evidence comes from observations of circumstellar envelopes which enshroud luminous AGB stars, and

may make them visible only in the infrared. The analysis of winds and circumstellar shells shows that mass loss rates range from $10^{-8}\,M_\odot$/year to $10^{-5}\,M_\odot$/year and are strongly correlated with increasing luminosity and decreasing effective temperature. The highest rates effectively terminate the AGB evolution by removing the envelope within several thousands of years to a level, where the star leaves the giant region (as in Fig. 34.1). In this phase, the stellar wind is often called a *superwind*, a term coined by Renzini in 1981, to indicate that it is orders of magnitudes higher than the standard Reimers wind (9.1). We will not go into the details of the observations and the physics of AGB winds, but give, as an illustrative example, a fit formula by van Loon et al. (2005) that describes the mass loss rate (in $M_\odot$/year) for oxygen stars (C/O < 1) as a function of the star's position in the HRD, and demonstrates the high sensitivity to effective temperature:

$$\log \dot{M}_{\rm AGB} = -5.65 + 1.05 \cdot \log\left(10^{-4}\frac{L}{L_\odot}\right) - 6.3 \cdot \log\left(\frac{T_{\rm eff}}{3500K}\right). \qquad (34.17)$$

Generally, it is believed that the winds of AGB stars are due to the coupling of the radiation field to dust forming in the outer atmospheres. The formation of dust is favoured by very low temperatures, which are achieved during and due to large-amplitude stellar pulsations (see Chap. 40). Indeed, many AGB stars are known to be pulsating stars of type Mira or semi-regular and long-period pulsators (periods are between 100 and 1,000 days). In addition, temperature variations during TPs also modulate the mass loss. The complex interplay between pulsating envelopes, the chemistry of dust formation, and the interaction with radiation poses an extremely difficult chemistry-radiation-hydrodynamics problem. So far, such models have been successful for carbon-rich atmospheres, and theoretical dust-driven wind models and mass loss rates are available for carbon stars. Again, as an example that is sufficient to make order-of-magnitude estimates for the mass loss rate, we give the fitting formula to theoretical carbon-dust models by Wachter et al. (2002):

$$\log \dot{M}_{\rm AGB} = -4.52 + 2.47 \cdot \log\left(10^{-4}\frac{L}{L_\odot}\right) - 6.81 \cdot \log\left(\frac{T_{\rm eff}}{2600K}\right) - 1.95 \cdot \log\left(\frac{M}{M_\odot}\right). \qquad (34.18)$$

Such fitting formulae may be accurate within one or two orders of magnitude. Within this accuracy, the similarity of the dependencies on L and $T_{\rm eff}$ in (34.17) and (34.18) is interesting. More about AGB mass loss can be found in the textbook by Habing and Olofsson (2003).

A more indirect but very convincing fact that demonstrates the importance of mass loss from AGB stars comes from the *initial-final-mass relation*, pioneered by Weidemann (1977; revised 2000). We describe briefly the general idea: spectrosopy of white dwarfs allows to determine surface gravity $g = GM/R$ and $T_{\rm eff}$. The

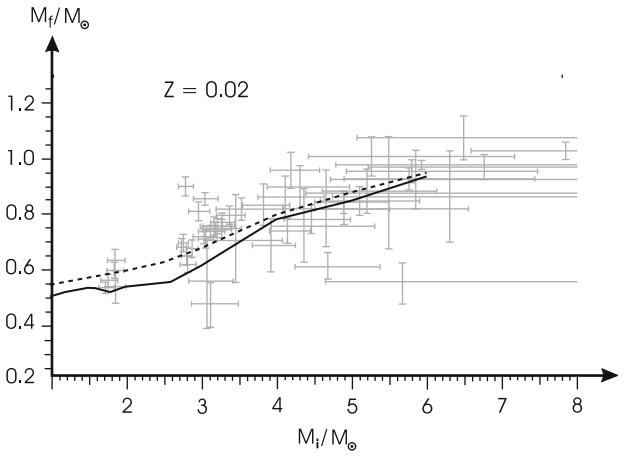

Fig. 34.7 The initial-final mass relation. The data points and their error bars are taken from Salaris et al. (2009). The *dashed line* is the empirical relation derived by Weidemann (2000). The *solid line* is the relation predicted from theoretical AGB evolution models for $Z = 0.02$ (After Weiss and Ferguson 2009)

former quantity, which can in principle also be determined from gravitational photon redshift, together with known mass-radius relations (Chap. 37) yields the white dwarf's mass. Theoretical cooling curves for the so determined mass, together with $T_{\rm eff}$, give the cooling age, $t_{\rm cool}$. If the white dwarfs are in a stellar cluster, the age t of this cluster can be determined from comparison with isochrones of appropriate composition. Since the white dwarfs are the descendants of former main-sequence stars in the cluster, the difference $t - t_{\rm cool}$ is the age the progenitor spent in the pre-white dwarf stages. This time is dominated by the main-sequence lifetime, which is depending on the initial mass, as we have estimated in (30.2) and plotted in Fig. 30.6. In this way, the initial mass can be determined. Since the more massive AGB stars and their mass loss are more interesting, open clusters of several 100 Myrs are mainly investigated. However, also binary systems, in which one component is a white dwarf, are suitable. A famous example is Sirius B; popular clusters are the Hyades, the Pleiades, and Praesepe.

Figure 34.7 shows the empirical initial-final-mass relation (Salaris et al. 2009; data points), the previous analytical fit by Weidemann (2000), and the prediction from theoretical AGB evolution (Weiss and Ferguson 2009), which included overshooting and mass loss according to (34.17) and (34.18). Within the errors the theoretical models lie well within the empirical data. This is an indication that the total mass loss is described well by the models. Notice that a $6\,M_\odot$ star ends as a white dwarf of only $1\,M_\odot$. It has lost a total of $5\,M_\odot$, and this happens mostly on the TP-AGB. The second remarkable result is that even for the highest masses ($\approx 8\,M_\odot$) the final white-dwarf mass is well below the critical Chandrasekhar mass

of $\approx 1.4\,M_\odot$. This will turn out to be an important fact in relation to the progenitors of supernovae (Chap. 36).

34.7 A Sample AGB Evolution

In this section, we will present the complete evolution of a star of $2\,M_\odot$ and a standard composition ($X = 0.695$, $Y = 0.285$, $Z = 0.02$) from the main-sequence until the final white-dwarf state. The calculations for this and many other values for mass and composition were done by A. Kitisikis (PhD thesis, Munich University, 2008) and published by Weiss and Ferguson (2009). They are the first attempt to include as many crucial physical aspects of AGB evolution as possible. Overshooting is treated according to (30.9), and applied at all convective boundaries. The opacity tables used include variations of C and O abundance and therefore are sensitive to dredge-up processes and in general lead to lower $T_{\rm eff}$ in case of carbon enhancement of the envelope due to the third dredge-up. Mass loss is included in parametrized form following (34.17) and (34.18), depending on the C/O ratio. Figure 34.8a gives an overview of the full evolution, and Fig. 34.8b shows the TP-AGB phase. Figure 34.9 summarizes details during the TPs.

The evolution starts on the main sequence, which lasts for 1.075 Gyr. A further 58 Myr are spent on the RGB, before helium ignites in a moderately energetic core helium flash, with a peak helium luminosity of "only" $\log L_{\rm He}/L_\odot = 7.2$. The surface luminosity of $\log L/L_\odot = 2.87$ is also lower than that of the RGB tip of low-mass stars indicating that at this mass, we are already in the transition region to intermediate-mass stars. Core helium burning, which lasts for 177 Myr, takes place in a barely visible loop around $\log L/L_\odot = 1.8$. Then the star starts to climb the E-AGB, and the first thermal pulses set in around $\log L/L_\odot = 3.0$. Figure 34.8b shows this part of the HRD in more detail. In the course of the TPs the peak luminosity increases and the effective temperature drops. This leads to stronger mass loss. The last TP, which sets in after C/O > 1 is reached, leads to a strong excursion to temperatures as low as 2,000 K. After this final pulse, due to the fast shedding of the envelope, the star contracts and crosses the HRD within 4,100 yrs. Its mass, and therefore the final white-dwarf mass, is $0.543\,M_\odot$. The E- and TP-AGB last for 15.4 and 2.6 Myr.

Details of the TP-AGB phase are given in Fig. 34.9. As mentioned in Sect. 34.3, an asymptotic pulse behaviour is slowly approached after about 10 TPs, but not completely reached, even after all 15 pulses. The first pulse is, as is very often found in such calculations, different from the subsequent ones. The surface luminosity drops more than for the $5\,M_\odot$ star of Fig. 34.3, due to the less massive envelope. However, it also shows a very short-lived peak of 500 'years' duration, which is not visible in Fig. 34.3. This is found in many models with massive envelopes and a deep penetration of the OCZ down to the hydrogen-burning shell.

Figure 34.9 also shows the interaction of dredge-up, effective temperature and mass loss. With increasing pulse number, the star gets increasingly cooler. At the

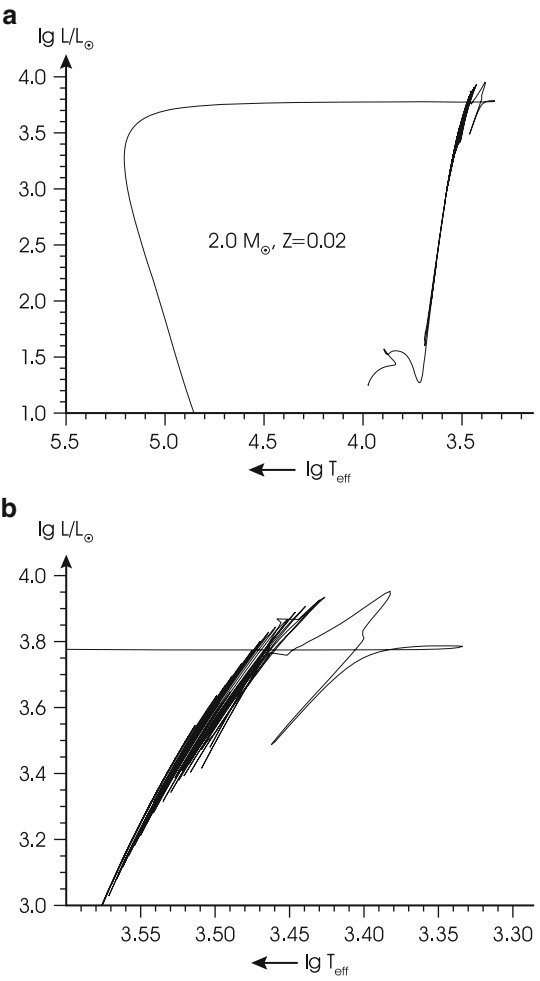

Fig. 34.8 (**a**) Evolution of a star of 2 $M_\odot$ and $Z = 0.02$ from the ZAMS to the white-dwarf cooling stage (Weiss and Ferguson 2009). (**b**) Detail view of the TP-AGB phase, with 15 TPs, the last one leading to an excursion to very low $T_{\rm eff}$, the final expulsion of the stellar envelope, and the beginning of the post-AGB transition to hot $T_{\rm eff}$ at nearly constant L. For details about the calculations, see text

same time, the carbon abundance in the envelope increases in each pulse due to dredge-up, ensured by the application of convective overshooting from the ISCZ.

The dredge-up in fact starts already with the first thermal pulse, but is interrupted until TP 9. Then a significant increase up to C/O $= 1$ takes place. Note that also some oxygen–the second result of helium burning–is dredged up. The increase in nitrogen is due to protons ingested from the envelope. The abundances in Fig. 34.9 are given in mass fractions, while the C/O ratio is in number fractions. This is the reason why the carbon abundance remains below that of oxygen, but C/O > 1 after pulse 14. At this moment, a strong increase in opacity due to the carbon-rich atmosphere leads to a drop in $T_{\rm eff}$, and thus, due to the high sensitivity of the mass loss rate to temperature, to a strong increase in $\dot{M}$. In the corresponding panel $\dot{M}$ increases to levels above $10^{-5}\,M_\odot/\text{year}$, such that the total mass (middle panel) is

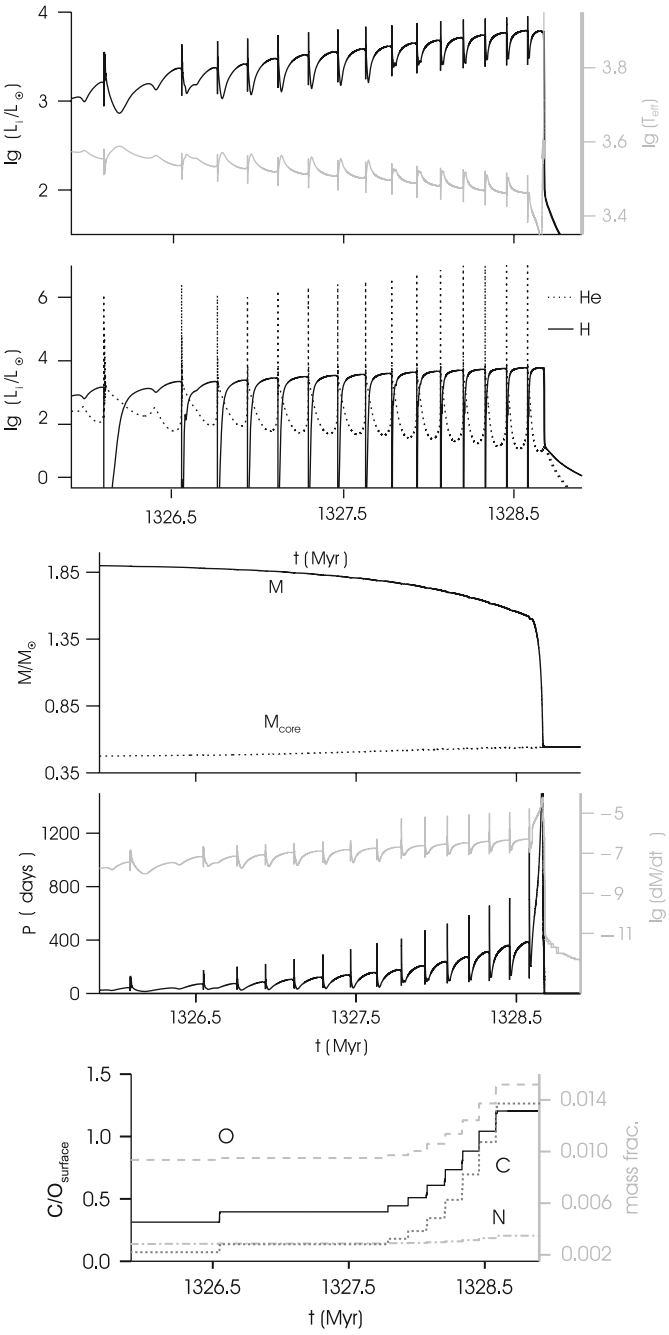

Fig. 34.9 Physical quantities during the TPs of the same model as in Fig. 34.8. The *panels* show, from *top* to *bottom*: total luminosity L (*left scale*) and $T_{\rm eff}$ (*right scale*); helium and hydrogen shell luminosity; total and C/O core mass; pulsation period (*left scale*) and mass loss rate (*right scale*); and finally C/O ratio at the surface (*left scale*) and C, N, and O mass fractions (*right scale*)

reduced to the core mass within 3.4×10^4 years. The pulsation period (second-to-last panel, left scale) is only a rough estimate and is needed only to decide when standard Reimers wind is replaced by (34.17) for C/O $<$ 1 or (34.18) for C/O $>$ 1. Dust-driven winds, for which large-amplitude pulsations are a necessary prerequisite (see Sect. 34.6), are taken into account only for periods longer than 400 days.

34.8 Super-AGB Stars

There is a small mass range between intermediate-mass and massive stars that may extend, depending on composition and author, from 7 to 12 $M_\odot$ or from $\approx$ 8 to 10 $M_\odot$, in which stars may ignite carbon burning off-centre under partially degenerate core conditions. Above the upper mass limit carbon ignites at the non-degenerate centre of stars, and below the lower mass limit, the core does not reach the necessary ignition temperature of about 7×10^8 K. To reach this temperature requires core masses in excess of $\approx 1\, M_\odot$, which, according to the empirical findings and theoretical predictions of the initial-final mass relation, (Fig. 34.7) is not obviously possible. Nevertheless, this option should not be excluded.

Siess (2006b, and reference therein) describes in detail the complicated evolution of such stars. The mass range, at a metallicity of $Z = 0.02$, is between 9 and 11.3 $M_\odot$. Here, we summarize only the main events in it. The carbon flash happens analogously to the helium flash we encountered earlier. It leads to a heating and expansion of the C/O core. However, these structural changes lead to a quenching of carbon burning, and core contraction is resumed. This now takes place under much less degenerate conditions, such that the core heats up and a second carbon ignition, in the literature called a "flame", sets in, and leads to central carbon burning. After this phase, which may last a few thousand years, carbon burning proceeds in a radiative shell around a neon-oxygen core. If it encounters carbon pockets around the core, convection zones may appear for some time.

There is also a number of convective episodes in the outer regions of the star. For example, the OCZ may reach the hydrogen-helium boundary before or during central carbon burning. This constitutes the second dredge-up we already know. It leads to the extinction of the hydrogen shell. The helium shell is providing most of the star's luminosity, and since the shell may be convective, in some stars, this convection zone may merge with the OCZ. As a result, the mass of the hydrogen-exhausted core is reduced substantially.

Carbon burning can also be quenched again due to strong cooling by neutrino losses such that after core carbon burning the He-shell is the only nuclear energy source of the star. Obviously, this shell is thermally unstable and will resume thermal pulses, during which the hydrogen is also reignited. This is the reason for the name super-AGB stars, as such stars share properties with AGB stars, but are more luminous. Since mass loss has to be minor in order to allow a sufficient core growth during the AGB phase, the envelope mass is still substantial and super-AGB stars may indeed suffer up to thousand TPs.

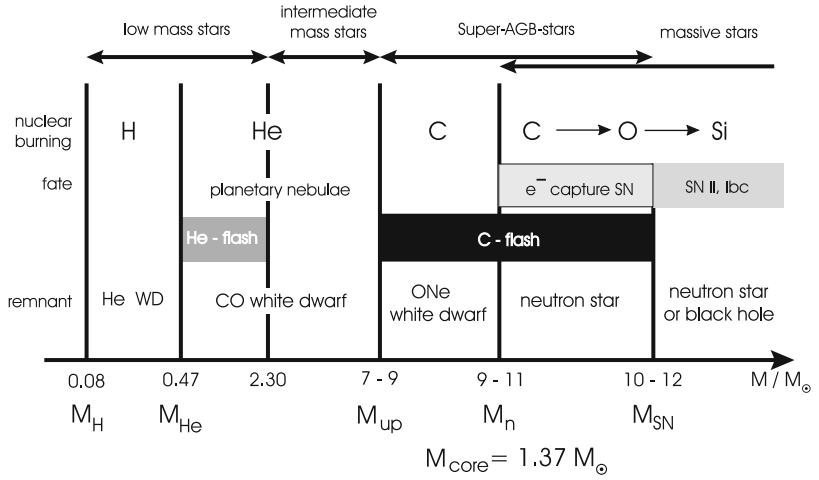

Fig. 34.10 Transition masses between different evolutionary paths for stars, and their final fate. $M_{\rm H}$, $M_{\rm He}$, $M_{\rm up}$, $M_{\rm n}$, and $M_{\rm SN}$ correspond to the minimum initial stellar mass for hydrogen, helium, and carbon ignition, the formation of a neutron star, and for stars undergoing a type II supernova explosion. The final fate of the star and its remnant are indicated for each mass range. Note that these mass limits depend crucially on the initial composition and on the detailed computations (After Siess 2006b)

The final fate of super-AGB stars depends on the mass of the NeO core. If it exceeds $\approx 1.37\,M_\odot$ after carbon burning, the nuclear evolution will go through all phases just as for massive stars. If it is slightly lower than this value initially, Ne ignition can be avoided and the core can grow due to shell burning and develop a highly degenerate NeO core of $1.37\,M_\odot$. It will not undergo the thermal pulses, but will end as a so-called *electron-capture supernova* (see Sect. 36.3.4), which is initiated by electron-capture reactions on ^{24}Mg, ^{24}Na, and other isotopes. This leads, among other effects, to the reduction of electron pressure, and a subsequent collapse of the core. A low-mass neutron star will be the remnant after the supernova explosion. If the NeO core mass always stays below this critical core mass, the star will end–after envelope expulsion–as a NeO white dwarf. In Fig. 34.10 an overview of the various mass limits separating the different evolutionary paths is given (adapted from Siess 2006b). These limits are very uncertain and depend a lot not only on the details of the computations, but also on the initial composition. In fact some limits may not even exist at all metallicities, because of effects of mass loss or overshooting.

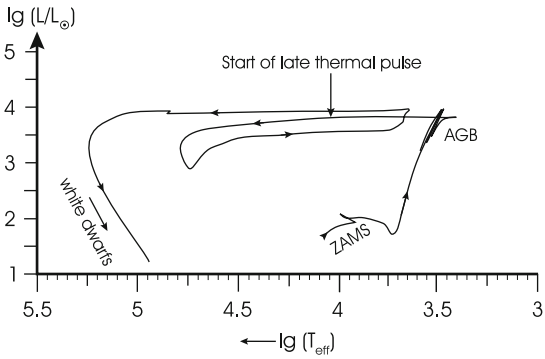

Fig. 34.11 Example for a *late thermal pulse* in a star of initially 2.7 $M_\odot$, according to Althaus et al. (2005)

34.9 Post-AGB Evolution

Stars of low and intermediate mass leave the AGB mainly due to the very short-lived superwind phase. Depending on the phase of the TP cycle this happens, the star may have a hydrogen- or helium-shell providing the majority of the total luminosity. The post-AGB stars are therefore divided into *hydrogen and helium burners*. The latter group generally has longer HRD-crossing timescales.

With increasing $T_{\rm eff}$, mass loss is quickly dying out. Depending on the density and expansion velocity of the circumstellar shell which was lost during the TP-AGB phase, the increasingly higher number of UV photons emerging from the star, which is crossing the HRD to very high temperatures, may ionize the circumstellar matter and lead to the creation of a planetary nebula. The critical values for $T_{\rm eff}$ are 30,000 K and 60,000 K for hydrogen and helium ionization. In addition, a hot wind with velocities of the order of 1,000 km/s ploughs into the slowly expanding shell (of a few tens of km/s), compressing it and creating shocks.

At the bluest point in the evolution (see Figs. 34.1 and 34.8), the shell is finally fading away and the star begins its final cooling phase and becomes a white dwarf.

However, in some cases, the star may still suffer a last thermal pulse. Such late pulses are found in numerical calculations both during the HRD crossing and during the earliest cooling phases. In the course of such a late TP the star returns to the AGB and resumes a second HRD crossing. We show such an excursion in the HRD in Fig. 34.11. Due to the mixing and burning episodes connected with the pulse the thin envelope undergoes drastic changes in its composition. In fact, there is a small number of stars which evolved drastically over a few decades including changes of the surface composition. These are generally connected with late TP events. Famous examples are Sakurai's object (V4334 Sgr), FG Sge, and V650 Aql. There is still a discrepancy between the timescales for the changes between the models and the objects, but this may be due to insufficient theories for time-dependent convection. This kind of objects and their relation to post-AGB evolution have been reviewed by Schönberner (2008).